Medical Engineering & Physics 33 (2011) 80–88

Contents lists available at ScienceDirect

Medical Engineering & Physics

journal homepage: www.elsevier.com/locate/medengphy

Simulation of abdominal aortic aneurysm growth with updating hemodynamic loads using a realistic geometry

A. Sheidaei[a], S.C. Hunley[a], S. Zeinali-Davarani[a], L.G. Raguin[a,b], S. Baek[a,*]

[a] Department of Mechanical Engineering, Michigan State University, East Lansing, MI 48824-1224, United States
[b] Department of Radiology, Michigan State University, East Lansing, MI 48824-1313, United States

ARTICLE INFO

Article history:
Received 19 April 2010
Received in revised form
10 September 2010
Accepted 16 September 2010

Keywords:
Vascular adaptation
Patient-specific model
Growth and remodeling
Fluid–solid-growth interaction

ABSTRACT

Advances in modeling vascular tissue growth and remodeling (G&R) as well as medical imaging usher in a great potential for integrative computational mechanics to revolutionize the clinical treatment of cardiovascular diseases. A computational model of abdominal aortic aneurysm (AAA) enlargement has been previously developed based on realistic geometric models. In this work, we couple the computational simulation of AAA growth with the hemodynamics simulation in a stepwise, iterative manner and study the interrelation between the changes in wall shear stress (WSS) and arterial wall evolution. The G&R simulation computes a long-term vascular adaptation with constant hemodynamic loads, derived from the previous hemodynamics simulation, while the subsequent hemodynamics simulation computes hemodynamic loads on the vessel wall during the cardiac cycle using the evolved geometry. We hypothesize that low WSS promotes degradation of elastin during the progression of an AAA. It is shown that shear stress-induced degradation of elastin elevates wall stress and accelerates AAA enlargement. Regions of higher expansion correlate with regions of low WSS. Our results show that despite the crucial role of stress-mediated collagen turnover in compensating the loss of elastin, AAA enlargement can be accelerated through the effect of WSS. The present study is able to account for computational models of image-based AAA growth as well as important hemodynamic parameters with relatively low computational expense. We suggest that the present computational framework, in spite of its limitations, provides a useful foundation for future studies which may yield new insight into how aneurysms grow and rupture.

1. Introduction

Understanding of the underlying processes that lead to the growth and structural weakening of an abdominal aortic aneurysm (AAA) is of critical importance in both diagnosis of the lesion progression and design of the patient-specific intervention. AAAs have been associated with local and systemic alterations of the aorta, influenced by age as well as genetic factors [1–3]. Marked reduction of the elastin content in AAA tissues has been reported in several studies [4–7]. It has been suggested that elastin degradation is attributed to the elevated activation of proteolytic matrix metalloproteinases (MMPs) that can be induced by various factors such as the abnormal distribution of wall shear stress (WSS) [8–11], inflammatory responses [12–14], and intraluminal thrombus formation [15,16]. Although it has been suggested that aneurysm growth is likely to occur in regions where the vessel wall is exposed to abnormally high/low WSS, the effect of WSS on the expansion rate of aneurysms is poorly understood. High WSS has been related to the initiation of cerebral aneurysms [17,18], whereas low shear has been associated with aneurysm progression [19], thrombus formation [20] and its rupture [18,21]. In this study, we test the hypothesis that an adverse decrease in WSS promotes elastin degeneration, and use computational simulations to track the possible time course of changes in the mechanical state of the aortic wall and its effects on processes governing the aneurysm expansion.

Although an AAA is often characterized by a thinning media with marked reduction of elastin, increasing evidence suggests that AAA formation is predominantly due to the growth and remodeling (G&R) of the aortic wall by collagen turnover [12,22,3]. Based on understandings of the ubiquitous role of mechano-regulated G&R of collagen in vascular adaptations, a number of computational models of (cerebral/aortic) aneurysm expansion have been developed where the stress/strain-mediated collagen turnover governs the expansion rate [23–29]. The previous computational models have been promising in improving our understanding of the underlying mechanisms involved in aneurysm enlargement. In the cerebral aneurysm model proposed in [24], collagen was assumed

* Corresponding author at: Department of Mechanical Engineering, 2457 Engineering Building, Michigan State University, East Lansing, MI 48824-1224, United States. Tel.: +1 517 432 3161.
E-mail address: sbaek@egr.msu.edu (S. Baek).

1350-4533/$ – see front matter © 2010 IPEM. Published by Elsevier Ltd. All rights reserved.
doi:10.1016/j.medengphy.2010.09.012

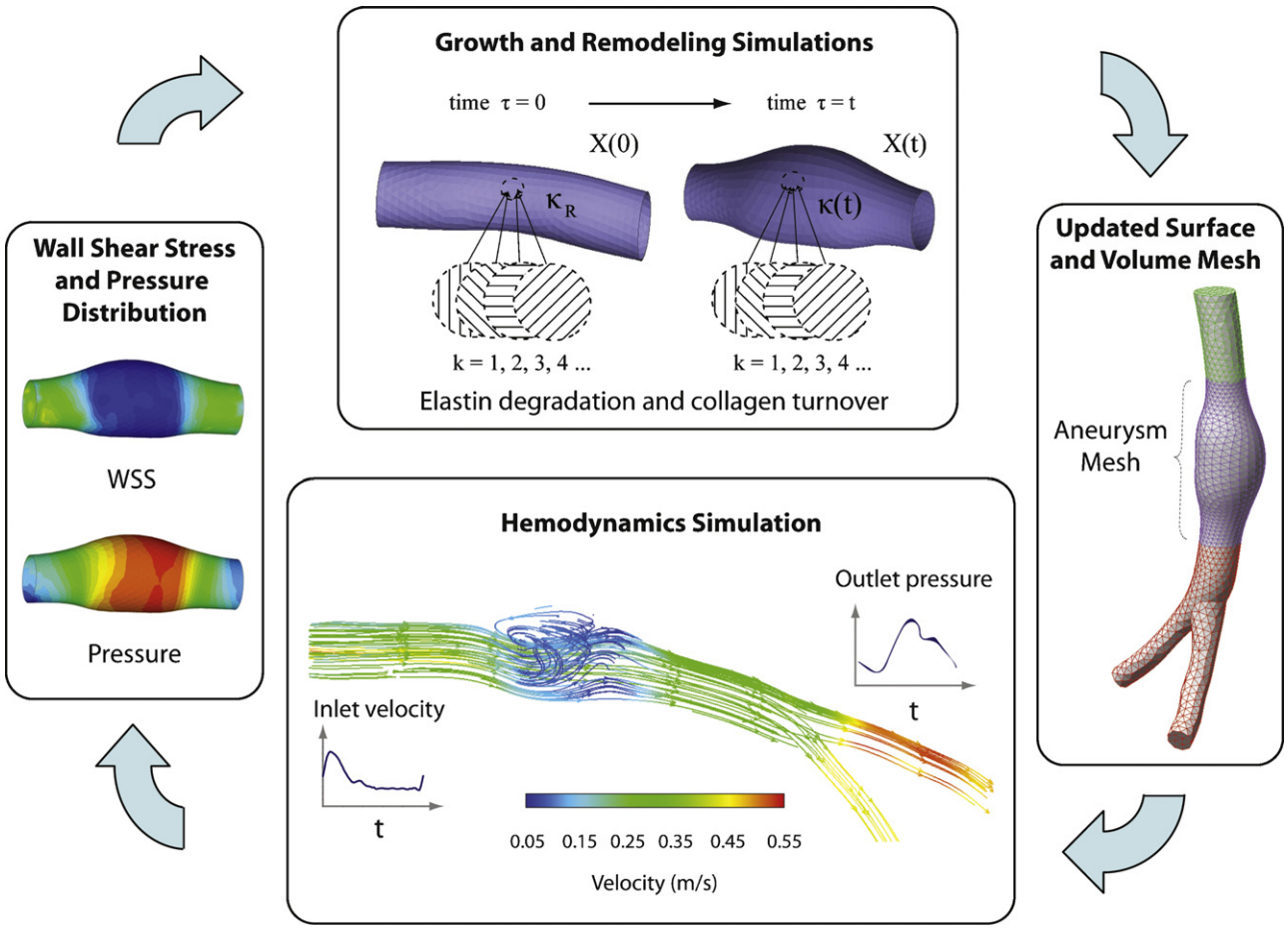

Fig. 1. Iterative loop and information transfer in the coupling between the hemodynamics and G&R simulations.

to be the only structural constituent responsible for the aneurysm enlargement [30,31]. However, elastin and smooth muscle (SM) cells are major components in abdominal aorta, and their continuous degradations and coupled interactions with stress-mediated collagen turnover are speculated to be the main cause for AAA enlargement. We employed a similar stress-mediated adaptation model and extended it to aortic aneurysms using an anatomically realistic geometry and studied the effect of spatial and temporal variations of elastin degradation on the intramural stress distribution and the subsequent aneurysm enlargement [32]. For clinical applications of these models, however, it is strongly desired to integrate the computational models of G&R with hemodynamics simulations to account for the role of hemodynamics variations. Recently, new computational frameworks that loosely couple vascular G&R simulation with hemodynamics simulation have been independently presented by Figueroa et al. [33] and Watton et al. [29], demonstrating their utility in modeling cerebral aneurysms using idealized geometries. In the present study, we employ the coupled framework by extending our previous AAA model [32] to simulate the evolution of an AAA while updating hemodynamic loads.

2. Methods

2.1. General computational framework

Following [33], we employ a fluid–solid-growth (FSG) simulation framework that utilizes loosely coupled iterations between short-term hemodynamics simulations and long-term G&R simulations, i.e., the hemodynamic loads on the vascular wall are updated in a stepwise manner as the AAA grows (Fig. 1). More specifically, in the iterative loop, the hemodynamics simulation computes blood flow during the cardiac cycle at a given time and the mechanical stimuli that affect vascular wall G&R (e.g., mean WSS and mean pressure) are extracted and transferred to the G&R simulations. The G&R simulation then simulates the evolution of the arterial wall over multiple time steps. When the shape of an AAA changes, the new shape is combined with extended (proximal and distal) regions and fed back to the hemodynamics simulation.

To simulate AAA enlargement, the central region of the abdominal aorta is used, and in order to obtain more accurate hemodynamic loads, the computational domain for the hemodynamics simulation is extended to the upper part of abdominal aorta (proximal side) and iliac branches (distal side). To characterize the hemodynamics within the blood vessel, unsteady blood flow is simulated within the reconstructed geometry using Fluent (Fluent Inc., Lebanon, NH, USA). A periodic velocity field corresponding to a prescribed inlet flow rate is used as an inlet boundary condition, and a periodic outlet back pressure is used as the outlet boundary condition. Lastly, the blood vessel is treated as having a rigid and impermeable wall.

Mean (time-averaged) WSS and the mean pressure are calculated for all nodes on the aneurysm wall over one cardiac cycle and transferred to the G&R simulation. The G&R part simulates the vessel wall adaptation accounting for elastin degradation and stress-mediated collagen turnover, both of which depend on the mechanical stimuli calculated from the hemodynamics simulation. For the G&R simulation, we use the finite element model of AAA enlargement developed by Zeinali-Davarani et al. [32], briefly described in the next section.

2.2. Constrained mixture model of arterial wall G&R

The arterial wall is assumed to be a thin membrane consisting of elastin, multiple families of collagen, and SM cells. Each constituent is produced and removed according to its turnover rate, which implies that constituents added at later times can have different stress-free configurations than those produced at earlier times [34]. It is assumed that the evolution of the mean configuration during the cardiac cycle is slow enough to be considered as a quasi-static process. Details of the finite element model of an AAA have been presented in [32]. Briefly, the strain energy w_R is postulated by

$$w_R(s) = \sum_{i=k,e,m} M_R^i(0)Q^i(s)\Psi^i(\mathbf{F}^i_{n(0)}(s)) + \int_0^s m_R^i(\tau)q^i(s,\tau)\Psi^i(\mathbf{F}^i_{n(\tau)}(s))d\tau, \quad (1)$$

where the superscripts k, e, and m represent the kth collagen fiber family, elastin, and SM, respectively. $M_R^i(0)$ is the areal mass density of constituent i in the healthy artery at time 0, $\mathbf{F}^i_{n(\tau)}(s)$ is the deformation gradient of constituent i that is produced at time τ corresponding to the mapping from its natural configuration to the current configuration at time s, $Q^i(s)$ is the fraction of the constituent i that was present at time 0 and still remains at time s, $m_R^i(\tau)$ is the true production rate of the constituent i at time τ per unit reference area, and $q^i(s,\tau)$ is its survival function, i.e., the fraction of constituent i produced at time τ that remains at time s. The strain energy functions for elastin, collagen, and passive SM are given as [33,32]

$$\Psi^e(\mathbf{F}^e_n) = \frac{c_1}{2}\left(c^e_{n[11]} + c^e_{n[22]} + \frac{1}{c^e_{n[11]}c^e_{n[22]} - {c^e_{n[12]}}^2} - 3\right) \quad (2)$$

$$\Psi^c(\mathbf{F}^k_n) = \frac{c_2}{4c_3}\{\exp[c_3({\lambda^k_{n(\tau)}}^2 - 1)^2] - 1\} \quad (3)$$

$$\Psi^m(\mathbf{F}^m_{n(\tau)}) = \frac{c_4}{4c_5}\{\exp[c_5({\lambda^m_{n(\tau)}}^2 - 1)^2] - 1\} \quad (4)$$

where $\mathbf{C}^e_n = {\mathbf{F}^e_n}^T\mathbf{F}^e_n$, $C^e_{n[11]}$, $C^e_{n[12]}$, and $C^e_{n[22]}$ are the components of $\mathbf{C}^e_n \cdot \lambda^k_{n(\tau)}$ and $\lambda^m_{n(\tau)}$ are the stretches of the fiber family k and SM produced at time τ. Even though the form of the strain energy function for SM is the same as collagen, its contribution to the passive mechanical properties of the wall is small [35]. The Cauchy membrane stress $\mathbf{T}$ is given by

$$\mathbf{T}(s) = \frac{2}{J(s)}\mathbf{F}(s)\frac{\partial w_R(s)}{\partial \mathbf{C}}\mathbf{F}(s)^T + \mathbf{T}_{act}(s). \quad (5)$$

The membrane stress due to the active SM tone is given as [36,37]

$$\mathbf{T}_{act}(s) = h^m(s)S_M\bar{\lambda}_2\left\{1 - \left(\frac{\bar{\lambda}_M - \bar{\lambda}_2}{\bar{\lambda}_M - \bar{\lambda}_0}\right)^2\right\}\mathbf{e}_2 \otimes \mathbf{e}_2 \quad (6)$$

where h^m is the current thickness of SM, S_M is the parameter for the vasoactive stress of SM, $\bar{\lambda}_2$ is the stretch of the SM cell, and $\bar{\lambda}_M$ and $\bar{\lambda}_0$ are the stretches corresponding to the maximum contraction and the active force generation limits, respectively.

2.3. Kinetics of elastin degradation and vascular adaptation in an AAA

It has been suggested that in AAAs, elastin degradation due to the activation of proteolytic enzymes [3] is likely to occur in regions where WSS is abnormally low [19,18]. However, the dose-dependence of elastin degradation kinetics with WSS is still unknown. For illustration purposes, similar to [29], we postulate a first order reaction equation for WSS (τ_w) where the survival fraction is given by

$$Q^e(s) = \exp(-\int_0^s K^e_d(\tau)d\tau), \quad (7)$$

where

$$K^e_d = \begin{cases} 0 & \tau_w \geq 0.8 \\ \frac{1}{2}K_{\max}\left[1 - \sin\frac{\pi}{4}(\tau_w - 0.6)\right] & 0.4 \leq \tau_w < 0.8 \\ K_{\max} & \tau_w \leq 0.4 \end{cases} \quad (8)$$

The functional form of elastin degradation is basically motivated by previous studies [18,29]. To date, no experimental studies have suggested the quantitative relationship between low WSS (e.g., <0.5 Pa) and elastin degradation, thus the range of values in Eq. (8) accounts for the possible variations with qualitatively reasonable outcome. We assume no elastin production during AAA evolution [38], whereas the production rates of collagen and SM depend on the intramural stress experienced by the resident cells given as [24]

$$m^i(s) = \frac{M_R(s)}{M_R(0)}\left(K^i_\sigma\left(\frac{\sigma^i(s)}{\sigma_h} - 1\right) + m^i_{basal}\right), \quad (9)$$

where

$$\sigma^k(s) = ||(\sum_k \gamma^k\boldsymbol{\sigma}^k(s))\mathbf{n}^k||, \quad \text{and} \quad \sigma^m(s) = ||\boldsymbol{\sigma}^m(s)\mathbf{n}^m||. \quad (10)$$

$\sigma^i(s)$ is a scalar measure of intramural stress, σ_h is the homeostatic stress value, K^i_σ is the parameter that controls stress-mediated G&R, and m^i_{basal} is the basal rate of mass production for the constituent i. γ^i, $\boldsymbol{\sigma}^i$ and $\mathbf{n}^i$ are the mass fraction, Cauchy stress and unit vector in the direction of the constituent i. The survival function for the constituent i is given as

$$q^i(s,\tau) = \exp(-\int_\tau^s K^c_d(\tilde{\tau})d\tilde{\tau}), \quad (11)$$

where $K^c_d(\tilde{\tau})$ is the rate of degradation at time $\tilde{\tau}$. The new collagen is deposited with a preferred alignment. Here, we assume that the alignment of the newly produced collagen is influenced by the orientation of the existing collagen and it consequently aligns towards the direction of the existing collagen family [39].

3. Computer simulations

3.1. Geometric model reconstruction and mesh generation

For patient-specific simulations, a 3-D model of a healthy aorta is constructed from MRI data of a healthy subject (image source: http://pubimage.hcuge.ch:8080/). SimVascular (Cardiovascular lab, Stanford University) software is used to construct a 3-D computational geometry from the MRI data (Fig. 2). Diameters for the inlet, the left and right common iliac arteries are measured to be roughly 14.5 mm, 8.6 mm and 7.6 mm, respectively.

The geometric model is then imported into Gambit (Lebanon, NH, USA). Using Boolean operations, the aneurysm region in the middle section of the 3-D model is isolated from the rest of the model. The fluid domain is meshed using tetrahedral/hybrid elements and the wall of the aneurysm section is meshed using triangular elements. The model consists of 37424 elements in the fluid domain and 4927 elements in the wall, of which 2744 are in the aneurysm section.

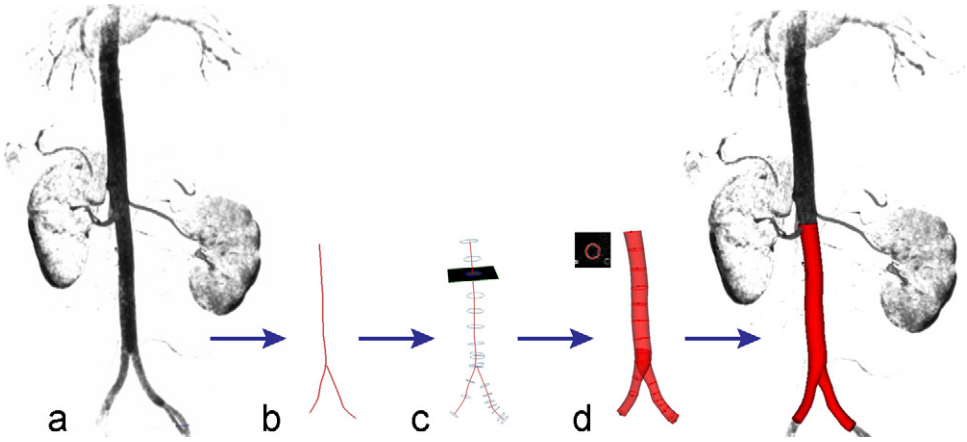

Fig. 2. Construction of a 3-D model of the aorta: (a) obtaining a magnetic resonance image of the abdominal aorta; (b) determination of vessel centerlines; (c) segmentation of the vessel lumens in each 2-D slice using level set methods; (d) combining the 2-D segmentations into a complete 3-D solid model of the aorta.

3.2. Hemodynamics simulation

A time-dependent velocity profile at the inlet and pressure waves at the outlets are prescribed in hemodynamics simulations based on data presented by Olufsen et al. [40] (Fig. 3). The cardiac cycle period is 0.94 s, with peak flow occurring at 0.24 s. Blood is treated as a homogenous, incompressible, Newtonian fluid [41,42]. Other properties are chosen based on standard values cited in the literature [43]; a dynamic viscosity of 0.0035 Pa·s, and a density of 1060 kg/m^3. Blood flow has been found to be laminar in AAAs, even during exercise [44]; thus, we assume laminar flow with a time-averaged Reynolds number as 563.

Fluent (ANSYS Inc., Lebanon, NH, USA) is used as a computational fluid dynamics (CFD) solver to solve the Navier–Stokes equations with specified boundary conditions. Each simulation runs for 7 cardiac cycles with a time step of 0.001 s, and then the CFD results for the last three cardiac cycles are averaged for each node. Finally, the mean WSS and pressure on the aneurysm wall are calculated to be used in the G&R simulation.

3.3. Simulation of a small AAA

Prior to AAA growth simulation, the vessel is assumed to be a healthy aorta, which represents an ideal maintenance state. In the ideal state, the rates of mass production and removal are balanced and the mechanical state for each constituent should be in homeostatic state. Hence, we need to prescribe the thickness and material properties such that homeostatic condition is satisfied for all constituents. As an initializing step, we approximate wall thickness and use the G&R simulation as an optimization tool to adapt into an equilibrium homeostatic state assuming four discrete collagen fiber families with alignments of 0°, 45°, 90°, −45° (see [33,32] for details). Immediately after initialization, the G&R simulation is initiated by introducing damage to the central section of the aorta on the concave side, where a fraction of elastin is removed instantaneously using an exponential distribution function (see Fig. 5, 300 days). In an iterative manner, values of mean WSS and pressure are updated and fed to the G&R simulation every 200 days, while the new shape after 200 days of G&R is combined with the extended regions and returned back into the hemodynamics simulation. The simulation period of 200 days is chosen based on comparatively slow observed changes in hemodynamic loads (mean pressure and WSS) when using 100-day periods, both of which result in the same AAA shapes observed in this work.

As stated earlier, in addition to the initial elastin damage, it is assumed that further degradation occurs during the G&R simulation and its rate is a function of WSS (namely "pressure–shear induced G&R"). To clearly show the contribution of WSS to AAA progression, we also simulate the G&R without WSS-induced elastin degradation (namely "pressure induced G&R") and compare the AAA growth rates over a total period of 2000 days of G&R. Table 1 summarizes the material parameters for each constituent used in our G&R simulation.

The absence of structurally significant elastin along with fewer SM cells has been widely observed in AAA tissues [45]. Moreover, the role of elastin in regulating SM migration, proliferation [46,47], apoptosis [48,49], and phenotype modulation [50] is recognized as well. To apply the same idea in our G&R model, the same form of damage considered for elastin is also applied to SM. Reducing the mass of SM in the constitutive relation affects the contribution of SM to the overall mechanical properties although its direct mechanical effect is comparatively smaller than other constituents [35].

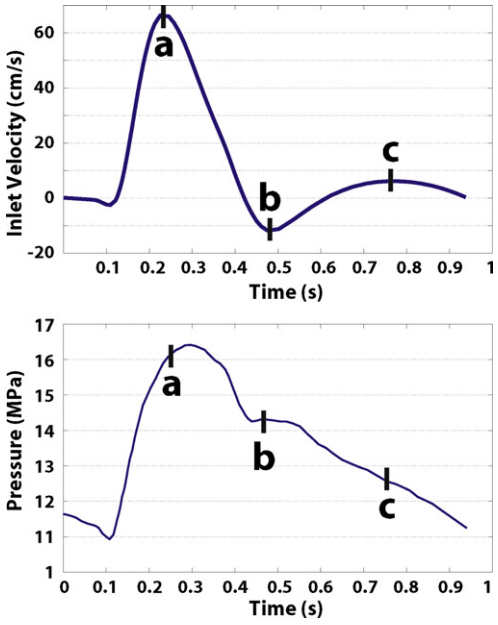

Fig. 3. Boundary conditions for the hemodynamics simulations: inlet velocity (top), outlet pressure (bottom) adapted from Olufsen et al. [40].

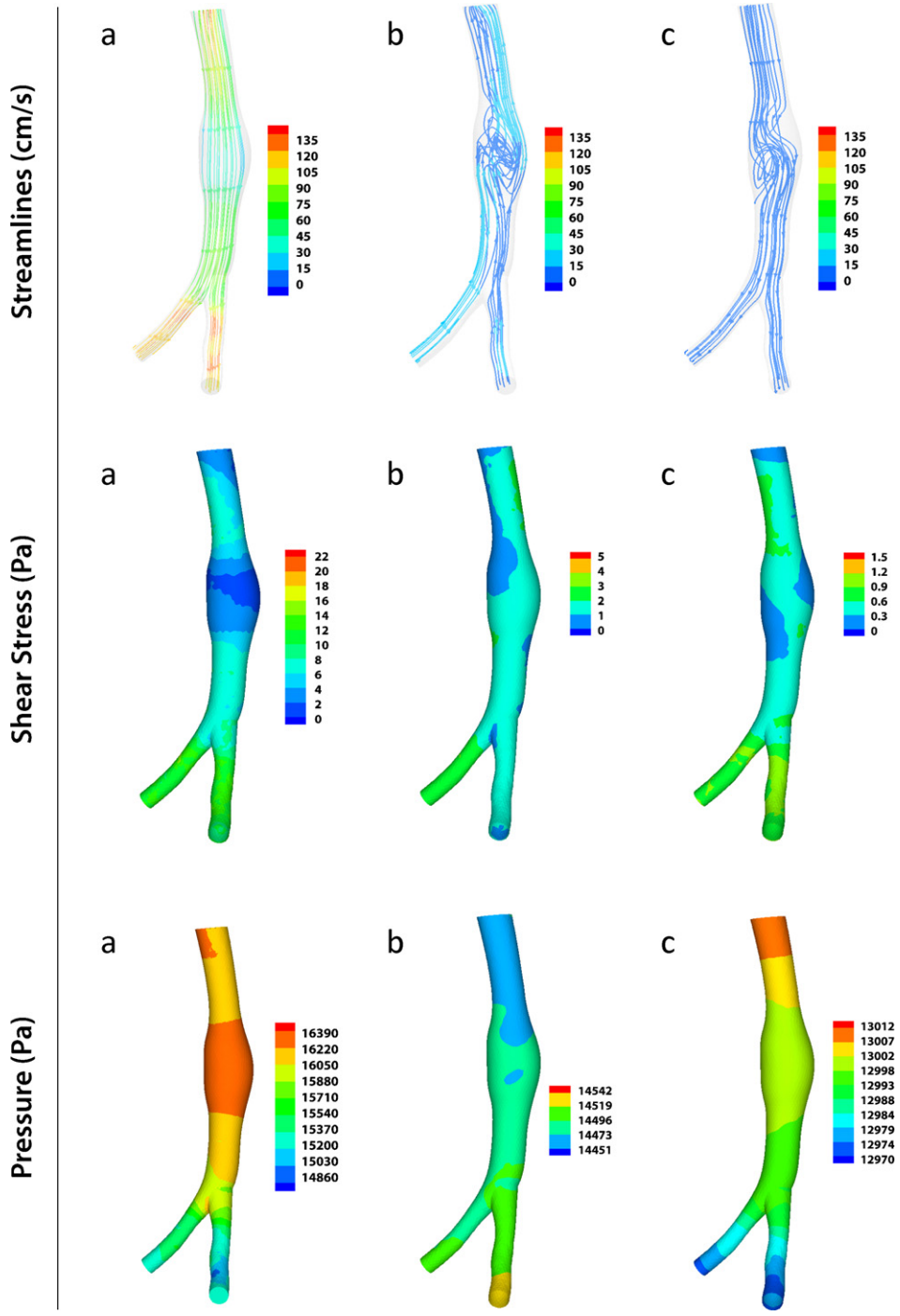

Fig. 4. Stream line, shear stress, and pressure at three different instances of the cardiac cycle (a–c in Fig. 3) after 1200 days of G&R.

4. Results

Fig. 4 shows the streamlines, WSS, and intramural pressure in a small AAA after 1200 days of G&R, at three different instances during the cardiac cycle, i.e., peak systole (a), end systole (b), and mid-diastole (c). The streamlines plots show areas of high velocity in branches of the distal aorta and low velocity in the region of greatest diameter in the AAA. Also, secondary flow is visible at (b) and (c) in the concavities of the aneurysm, while no recirculation is observed at (a), suggesting that in the early stages of an AAA, blood flow is still able to wash platelets away from the arterial wall.

As shown in Fig. 5, introducing an initial damage on the concave side causes a small bulge at this location, altering the hemodynamics, and leading to the gradual expansion of the vessel wall on the opposite side (i.e., convex side), where more reduction in WSS occurs. Similar to Watton et al. [29], elastin concentration correlates well with the WSS distribution as the lesion expands. The range of mean WSS on the aneurysmal wall is from 0 to 2.2 Pa, similar to the range found in [41].

Fig. 6 shows the distribution of maximum principal stress for pressure–shear induced G&R and pressure induced G&R at different times. For pressure–shear induced G&R, the maximum principal stress is observed to be slightly higher than that for pressure

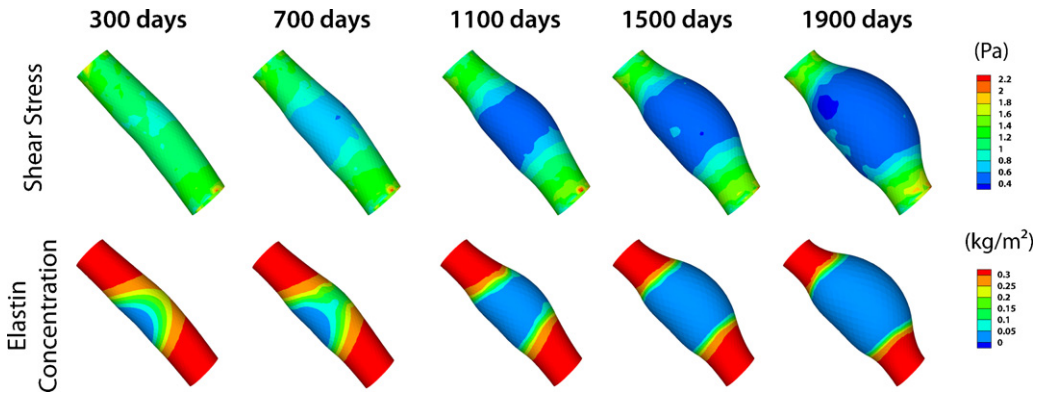

Fig. 5. Distribution of the wall shear stress (top) and elastin concentration (bottom) within an enlarging aneurysm during G&R process.

Table 1
Constitutive and kinetics parameters for each constituents used in G&R simulations.

Elastin	$c_1 = 112\,\text{Pa/kg}$, $K_{\max} = 0.02$
Collagen	$c_2 = 917\,\text{Pa/kg}$, $c_3 = 25.0$, $\sigma_h = 135\,\text{kPa}$, $K_d^c = 0.02$, $K_\sigma^k / m_{basal}^k = 0.05$
Smooth muscle	$c_4 = 26.9\,\text{Pa/kg}$, $c_5 = 8.5$, $S_M = 42\,\text{kPa}$, $\bar{\lambda}_M = 1.2$, $\bar{\lambda}_0 = 0.7$, $K_\sigma^m / m_{basal}^m = 0.05$

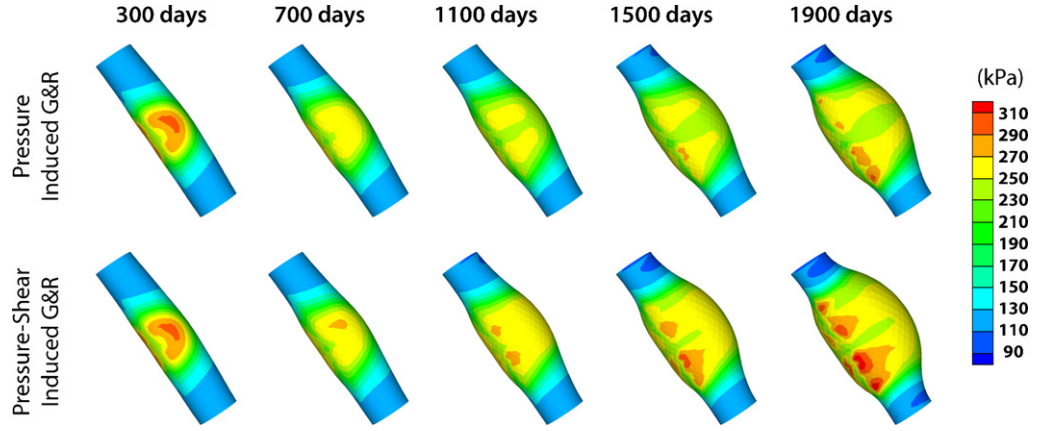

Fig. 6. Distribution of the maximum principal stress (kPa) during aneurysm enlargement; Comparison between pressure induced G&R (top) and pressure–shear induced G&R (bottom).

induced G&R during the aneurysm development. Also note that in both simulations, the peak value of the maximum principal stress apparently decreases until 900 days of G&R after which it monotonically increases.

The results of the pressure induced G&R simulations with or without updated pressure were similar. In other words, mean pressure did not change significantly during the aneurysm growth (<1% change in the mean pressure after 1500 days of G&R). In Fig. 7, the collagen (areal) densities are compared between pressure induced G&R and pressure–shear induced G&R. Because we assume that collagen production is a function of stress, areas with high principal stress correspond to areas of high collagen densities, as can be observed when comparing Figs. 6 and 7. To supplement this observation, the collagen densities around the midsection of the

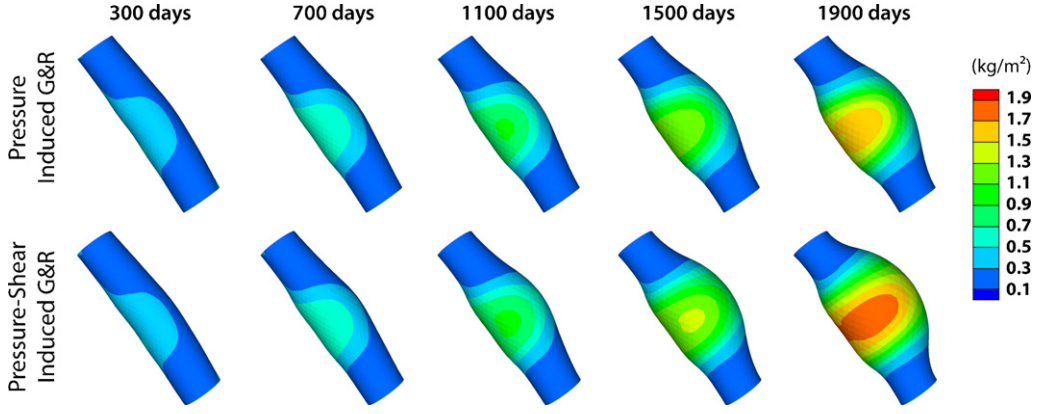

Fig. 7. Distribution of collagen density (kg/m^2) during aneurysm enlargement; comparison between pressure induced G&R (top) and pressure–shear induced G&R (bottom).

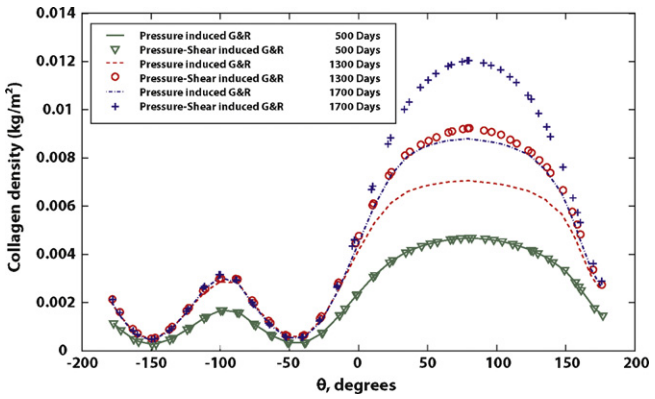

Fig. 8. Distribution of collagen density around the AAA midsection during aneurysm enlargement; Comparison between pressure induced G&R and pressure–shear induced G&R.

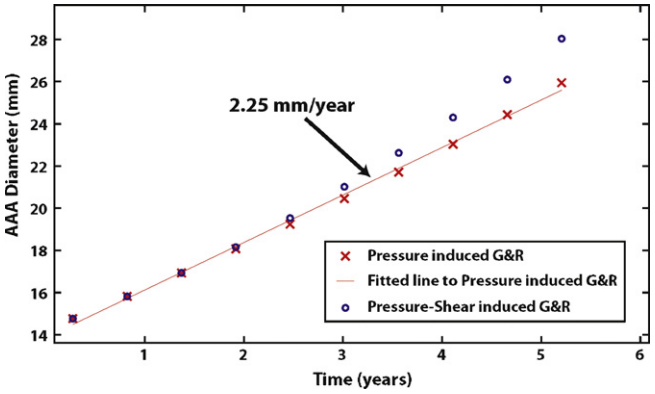

Fig. 9. Expansion rates of the simulated AAA; comparison between pressure induced G&R and pressure–shear induced G&R.

vessel for pressure–shear induced G&R and pressure induced G&R are plotted in Fig. 8. The difference between the pressure induced growth and the pressure–shear induced growth appears negligible up until 500 days of aneurysm growth, after which significant differences can be observed as time further progresses (Fig. 8). The distribution trend of collagen, elastin, and WSS along the vessel with respect to time is consistent with Watton et al. [29].

Fig. 9 shows the aneurysm expansion rates for both pressure induced and pressure–shear induced G&R simulations. Pressure induced G&R follows a linear trend with an expansion rate of 2.25 mm/year, while pressure–shear induced enlargement deviates from this linear trend after 3 years. These results are well within the range of reported expansion rates for small AAAs in clinical follow-up studies, e.g., 2.2–5.7 mm/year [51], 2.6–3.2 mm/year [52], 2.1 mm/year [53], 3 mm/year [54].

5. Discussion

In this study, we presented a framework that iteratively computes stress-mediated vascular G&R and blood flow based on a realistic geometry. Using coupled simulations the solid module accounted for altered hemodynamic loads during vascular G&R and simulated the gradual expansion of a lesion during the early period of an AAA (<3 cm), while the fluid module simulated blood flow with updated geometries. We found that mean WSS gradually decreases in the lesion during the expansion, as expected, and hypothesized that low WSS augments the pathological condition of the aneurysmal region [55,56]. The present study demonstrated the effects of low WSS induced elastin degradation on AAA progression through increasing its expansion rate, consistent with suggestions from hemodynamics studies using patient-specific models [19,57]. Platt et al. [58] demonstrated that elastinolytic proteases such as cathespin L are inhibited at WSS values of 1.5 Pa under laminar shear flow, whereas areas of low, oscillatory WSS ($\pm$5 dynes/cm^2 = 0.5 Pa) enhance the activity of cathespin L, resulting in elastin degradation. This is consistent with other hypotheses that low WSS (<1.5 Pa) leads to the apoptosis of the endothelial cells and promote aneurysm growth [29]. Nevertheless, our pressure–shear induced G&R simulation showed that when most of the elastin is degraded (e.g., after 1900 days), the AAA expansion is only about 10% greater than that of the pressure induced G&R (Fig. 9). Despite the possibility of exponential enlargement due to additional elastin degradation, the results imply that collagen can play a significant role in compensating for the loss of elastin [27] and controlling the expansion rate of aneurysms [24,32]. It is endorsed by marked increase of collagen content in the belly of aneurysm (Figs. 7 and 8), consistent with clinical observations by Menashi et al. [6]. Typically, AAAs enlarge continuously, implying that the stress-mediated collagen turnover may compensate for a local elevation of intramural stress, but not enough to stabilize growth. Our results support this claim by showing that the peak stress induced by the elastin damage gradually decreases, but the average stress level increases as the aneurysm expands (Fig. 6).

Similar to Watton and Hill [27], our preliminary tests showed that the expansion rate of the aneurysm is sensitive to the collagen half-life. That is, an aneurysm expands more quickly with a shorter collagen half-life and expands more slowly with a longer collagen half-life. The collagen half-life in an arterial wall is 60–70 days under normal physiological conditions, but can be reduced to 17 days in pathological conditions [59]. In our simulation, the collagen half-life was set to about 35 days. Variation of the stress-mediation parameter, K_σ, has a direct impact on the aneurysm expansion rate [32] via competition between local thickening and overall radial expansion of the lesion [23,24]. However, the collagen half-life and stress-mediation parameters were taken as constant values during the evolution of aneurysms, whereas they may change between individuals as well as during growth of an AAA, depending on physiological and pathological conditions. To account for multifactorial and dynamic changes of turnover parameters, more studies are needed to quantify these pathological changes during an AAA evolution.

Although we did not directly relate the kinetics of collagen turnover to WSS, findings from this study advocate further investigation of the influence of WSS on the collagen turnover during aneurysm expansion. It has been observed that endothelin-1 (ET-1) is upregulated in response to decreased shear [60], prompting collagen synthesis by SM cells [61]. Although these events imply an increase in collagen production during aneurysm expansion, proteolytic activities may also increase by low WSS through macrophage adhesion and inflammation [62,11]. Apparently, the imbalance between collagen production and removal is conducive to the growth and rupture of the lesion. It also appears that the interactions between SM and endothelial cells may influence the endothelial response to WSS [62], whereas the role of SM cells can be altered by apoptosis [48,49] and phenotype modulation [50]. Although overall contribution of SM cells to the arterial wall mechanical properties is not significant relative to other components [35], they indeed play a crucial role in regulating extracellular matrix turnover through its mechanosensitive characteristics [63–67] as well as its interaction with endothelial cells in shear-modulated collagen production [61]. There is a pressing need for supplementary clinical data to enhance our understanding of these combined effects and build better models that account for multifaceted and multiscale processes.

In their function form of elastin degradation, Watton et al. [29] assumed 0.5 Pa and 2 Pa as the critical values of WSS, consistent

with observations by [18]. Instead, we postulated a first order kinetic equation along with a sinusoidal function of WSS where 0.6 is assumed to be the midpoint (Eqs. (7) and (8)). The outcome of the specific form of elastin degradation considered in this study was consistent with [29] as they assumed full elastin degradation for WSS values of 0.5 Pa and lower. Fig. 5 demonstrates that after 1100 days of G&R a considerable region of the wall is experiencing low WSS ($\leq$0.6 Pa), resulting in a relatively large area of elastin degradation around the circumference (Fig. 5). This corresponds well with the time that the lesion enlargement starts to accelerate (3 years in Fig. 9). As the lesion grows further (e.g., at 1900 days of G&R), the region of low WSS ($\leq$0.6 Pa) spreads out resulting in a complete removal of elastin along the lesion (Fig. 5). These results are consistent with [18] who found low WSS values (<0.5 Pa) at the tip of ruptured aneurysms. To the author's knowledge, no study has suggested a specific functional form for the relation between WSS and elastin degradation. The form considered in this study, nonetheless, showed reasonable simulation results.

There are several limitations associated with the current model. The geometric model in our simulation used images from a healthy aorta. When the image is obtained from an AAA patient in advanced stages, however, one requires more information about the *in vivo* properties and pathological conditions to be incorporated in the current computational model. In this study, the initial damage of elastin represents the initial weakening of the aortic wall due to pathogenesis which is not yet completely understood. Understanding the extent of damage to elastin and SM required for an aneurysm to be initiated in pathogenic conditions needs more studies with experimental validations. The shape of the damage was relatively simple, whereas Zeinali-Davarani et al. [32] simulated the evolution of AAAs without considering hemodynamics variations and compared different spatial and temporal shapes of elastin damage. Interestingly, they also found that aneurysms enlarged on the convex side although damage was introduced on the concave side of the artery, which was attributed to the changes in intramural stress during the G&R process. It appears that the geometry of the artery affects AAA enlargement through both alteration of hemodynamics [17] and intramural stress distribution [68,69], reiterating the importance of patient-specific geometric models of AAAs.

We did not account for oscillatory effects of WSS, whereas the WSS reversal has been shown to correlate with aneurysm formation [70]. Himburg et al. [71] suggested that endothelial proinflammatory gene expression is most sensitive to oscillatory shear with low mean and reversing conditions, an observation supported by other studies [72–74]. Moreover, coexisting high and low shear regions, present in aneurysms [41,18] can also activate platelets and allow their deposition on the endothelial surface, leading to thrombosis formation [20].

Finally, the most challenging task in patient-specific models of AAA expansion will be incorporating the effects of intraluminal thrombus and perivascular tissues. It has been suggested that the intraluminal thrombus layer plays an important role in expansion and rupture of advanced aneurysms through direct mechanical [75] as well as indirect chemomechanical effects [15,16]. Hence, the current study represents the early stages of AAA expansion without the intraluminal thrombus layer. In spite of its limitations, we suggest that the present computational framework provides a useful foundation for future studies towards further understanding of the aneurysm growth and rupture.

Acknowledgements

We gratefully acknowledge Dr. J.D. Humphrey at Texas A&M University and Drs. C.A. Taylor and C.A. Figueroa at Stanford University for valuable discussions.

Conflict of interest statement

The authors of this paper do not have conflict of interest with other organizations to publish these results in the Medical Engineering & Physics.

References

[1] Baxter BT, Davis VA, Minion DJ, Wang YP, Lynch TG, McManus BM. Abdominal aortic-aneurysms are associated with altered matrix proteins of the nonaneurysmal aortic segments. Journal of Vascular Surgery 1994;19:797–803.
[2] Goodall S, Crowther M, Hemingway DM, Bell PR, Thompson MM. Ubiquitous elevation of matrix metalloproteinase-2 expression in the vasculature of patients with abdominal aneurysms. Circulation 2001;104:304–9.
[3] Powell JT. Abdominal aortic aneurysm. In: An introduction to vascular biology. Cambridge University Press; 2002. p. 318–26.
[4] Campa JS, Greenhalgh RM, Powell JT. Elastin degradation in abdominal aortic-aneurysms. Atherosclerosis 1987;65:13–21.
[5] He CM, Roach MR. The composition and mechanical-properties of abdominal aortic-aneurysms. Journal of Vascular Surgery 1994;20:6–13.
[6] Menashi S, Campa JS, Greenhalgh RM, Powell JT. Collagen in abdominal aortic-aneurysm—typing content, and degradation. Journal of Vascular Surgery 1987;6:578–82.
[7] Sumner DS, Hokanson DE, Strandness DEJ. Stress strain characteristics and collagen elastin content of abdominal aortic aneurysms. Surgery Gynecology and Obstetrics 1970;130:459–66.
[8] Hoshina K, Sho E, Sho M, Nakahashi TK, Dalman RL. Wall shear stress and strain modulate experimental aneurysm cellularity. Journal of Vascular Surgery 2003;37:1067–74.
[9] Miller FJ. Aortic aneurysms—it's all about the stress. Arteriosclerosis Thrombosis and Vascular Biology 2002;22:1948–9.
[10] Nakahashi TK, Hoshina K, Tsao PS, Sho E, Sho M, Karwowski JK, et al. Flow loading induces macrophage antioxidative gene expression in experimental aneurysms. Arteriosclerosis Thrombosis and Vascular Biology 2002;22:2017–22.
[11] Sho E, Sho M, Hoshina K, Kimura H, Nakahashi TK, Dalman RL. Hemodynamic forces regulate mural macrophage infiltration in experimental aortic aneurysms. Experimental and Molecular Pathology 2004;76:108–16.
[12] Choke E, Cockerill G, Wilson WRW, Sayed S, Dawson J, Loftus I, et al. A review of biological factors implicated in abdominal aortic aneurysm rupture. European Journal of Vascular and Endovascular Surgery 2005;30:227–44.
[13] Middleton RK, Lloyd GM, Bown MJ, Cooper NJ, London NJ, Sayers RD. The pro-inflammatory and chemotactic cytokine microenvironment of the abdominal aortic aneurysm wall: a protein array study. Journal of Vascular Surgery 2007;45:574–80.
[14] Shimizu K, Mitchell RN, Libby P. Inflammation and cellular immune responses in abdominal aortic aneurysms. Arteriosclerosis Thrombosis and Vascular Biology 2006;26:987–94.
[15] Fontaine V, Jacob MP, Houard X, Rossignol P, Plissonnier D, Angles-Cano E, et al. Involvement of the mural thrombus as a site of protease release and activation in human aortic aneurysms. American Journal of Pathology 2002;161:1701–10.
[16] Vorp DA, Lee PC, Wang DHJ, Makaroun MS, Nemoto EM, Ogawa S, et al. Association of intraluminal thrombus in abdominal aortic aneurysm with local hypoxia and wall weakening. Journal of Vascular Surgery 2001;34:291–9.
[17] Hoi YM, Meng H, Woodward SH, Bendok BR, Hanel RA, Guterman LR, et al. Effects of arterial geometry on aneurysm growth: three-dimensional computational fluid dynamics study. Journal of Neurosurgery 2004;101:676–81.
[18] Shojima M, Oshima M, Takagi K, Torii R, Hayakawa M, Katada K, et al. Magnitude and role of wall shear stress on cerebral aneurysm—computational fluid dynamic study of 20 middle cerebral artery aneurysms. Stroke 2004;35:2500–5.
[19] Boussel L, Rayz V, McCulloch C, Martin A, Acevedo-Bolton G, Lawton M, et al. Aneurysm growth occurs at region of low wall shear stress patient-specific correlation of hemodynamics and growth in a longitudinal study. Stroke 2008;39:2997–3002.
[20] Bluestein D, Niu L, Schoephoerster RT, Dewanjee MK. Steady flow in an aneurysm model: correlation between fluid dynamics and blood platelet deposition. Journal of Biomechanical Engineering-Transactions of the ASME 1996;118:280–6.
[21] Valencia A, Morales H, Rivera R, Bravo E, Galvez M. Blood flow dynamics in patient-specific cerebral aneurysm models: The relationship between wall shear stress and aneurysm area index. Medical Engineering & Physics 2008;30:329–40.
[22] Kratzbery JA, Walker PJ, Rikkers E, Raghavan ML. The effect of proteolytic treatment on plastic deformation of porcine aortic tissue. Journal of the Mechanical Behavior of Biomedical Materials 2009;2:65–72.
[23] Baek S, Rajagopal KR, Humphrey JD. Competition between radial expansion and thickening in the enlargement of an intracranial saccular aneurysm. Journal of Elasticity 2005;80:13–31.
[24] Baek S, Rajagopal KR, Humphrey JD. A theoretical model of enlarging intracranial fusiform aneurysms. Journal of Biomechanical Engineering-Transactions of the ASME 2006;128:142–9.
[25] Kroon M, Holzapfel GA. A model for saccular cerebral aneurysm growth by collagen fibre remodelling. Journal of Theoretical Biology 2007;247:775–87.

[26] Kroon M, Holzapfel GA. A theoretical model for fibroblast-control led growth of saccular cerebral aneurysms. Journal of Theoretical Biology 2009;257:73–83.
[27] Watton PN, Hill NA. Evolving mechanical properties of a model of abdominal aortic aneurysm. Biomechanics and Modeling in Mechanobiology 2009;8:25–42.
[28] Watton PN, Hill NA, Heil M. A mathematical model for the growth of the abdominal aortic aneurysm. Biomechanics and Modeling in Mechanobiology 2004;3:98–113.
[29] Watton PN, Raberger NB, Holzapfel GA, Ventikos Y. Coupling the hemodynamic environment to the evolution of cerebral aneurysms: computational framework and numerical examples. Journal of Biomechanical Engineering-Transactions of the ASME 2009;131, article no. 101003.
[30] Bruno G, Todor R, Lewis I, Chyatte D. Vascular extracellular matrix remodeling in cerebral aneurysms. Journal of Neurosurgery 1998;89:431–40.
[31] Gaetani P, Tartara F, Grazioli V, Tancioni F, Infuso L, Baena RR. Collagen cross-linkage, elastolytic and collagenolytic activities in cerebral aneurysms: a preliminary investigation. Life Science 1998;63:285–92.
[32] Zeinali-Davarani S., Sheidaei A., Baek S. A finite element model of stress-mediated vascular adaptation: application to abdominal aortic aneurysms. Computer Methods in Biomechanics and Biomedical Engineering, in press, doi:10.1080/10255842.2010.495344.
[33] Figueroa CA, Baek S, Taylor CA, Humphrey JD. A computational framework for fluid–solid-growth modeling in cardiovascular simulations. Computer Methods in Applied Mechanics and Engineering 2009;198:3583–602.
[34] Humphrey JD, Rajagopal KR. A constrained mixture model for growth and remodeling of soft tissues. Mathematical Models & Methods in Applied Sciences 2002;12:407–30.
[35] Burton AC. Relation of structure to function of the tissues of the wall of blood vessels. Physiological Reviews 1954;34:619–42.
[36] Baek S, Valentin A, Humphrey JD. Biochemomechanics of cerebral vasospasm and its resolution: II. Constitutive relations and model simulations. Annals of Biomedical Engineering 2007;35:1498–509.
[37] Rachev A, Hayashi K. Theoretical study of the effects of vascular smooth muscle contraction on strain and stress distributions in arteries. Annals of Biomedical Engineering 1999;27:459–68.
[38] Cardamone L, Valentin A, Eberth JF, Humphrey JD. Origin of axial prestretch and residual stress in arteries. Biomechanics and Modeling in Mechanobiology 2009;8:431–46.
[39] Wang JHC, Jia F, Gilbert TW, Woo SLY. Cell orientation determines the alignment of cell-produced collagenous matrix. Journal of Biomechanics 2003;36:97–102.
[40] Olufsen MS, Peskin CS, Kim WY, Pedersen EM, Nadim A, Larsen J. Numerical simulation and experimental validation of blood flow in arteries with structured-tree outflow conditions. Annals of Biomedical Engineering 2000;28:1281–99.
[41] Finol EA, Amon CH. Flow dynamics in anatomical models of abdominal aortic aneurysms: computational analysis of pulsatile flow. Acta Cientifica Venezolana 2003;54:43–9.
[42] Perktold K, Resch M, Florian H. Pulsatile non-Newtonian flow characteristics in a 3-dimensional human carotid bifurcation model. Journal of Biomechanical Engineering-Transactions of the ASME 1991;113:464–75.
[43] Berger SA, Goldsmith W, Lewis ER. Introduction to bioengineering. Oxford, UK: Oxford University Press; 2000.
[44] Egelhoff CJ, Budwig RS, Elger DF, Khraishi TA, Johansen KH. Model studies of the flow in abdominal aortic aneurysms during resting and exercise conditions. Journal of Biomechanics 1999;32:1319–29.
[45] Carmo M, Colombo L, Bruno A, Corsi FRM, Roncoroni L, Cuttin MS, et al. Alteration of elastin, collagen and their cross-links in abdominal aortic aneurysms. European Journal of Vascular and Endovascular Surgery 2002;23:543–9.
[46] Karnik SK, Brooke BS, Bayes-Genis A, Sorensen L, Wythe JD, Schwartz RS, et al. A critical role for elastin signaling in vascular morphogenesis and disease. Development 2003;130:411–23.
[47] Li DY, Brooke B, Davis EC, Mecham RP, Sorensen LK, Boak BB, et al. Elastin is an essential determinant of arterial morphogenesis. Nature 1998;393:276–80.
[48] Lopez Candales A, Holmes DR, Liao SX, Scott MJ, Wickline SA, Thompson RW. Decreased vascular smooth muscle cell density in medial degeneration of human abdominal aortic aneurysms. American Journal of Pathology 1997;150:993–1007.
[49] Thompson RW, Liao SX, Curci JA. Vascular smooth muscle cell apoptosis in abdominal aortic aneurysms. Coronary Artery Disease 1997;8:623–31.
[50] Ailawadi G, Moehle CW, Pei H, Walton SP, Yang ZQ, Kron IL, et al. Smooth muscle phenotypic modulation is an early event in aortic aneurysms. Journal of Thoracic and Cardiovascular Surgery 2009;138:1392–9.
[51] Sterpetti AV, Schultz RD, Feldhaus RJ, Cheng SE, Peetz DJ. Factors influencing enlargement rate of small abdominal aortic-aneurysms. Journal of Surgical Research 1987;43:211–9.
[52] Baxter BT, Terrin MC, Dalman RL. Medical management of small abdominal aortic aneurysms. Circulation 2008;117:1883–9.
[53] Nevitt MP, Ballard DJ, Hallett JW. Prognosis of abdominal aortic-aneurysms—a population-based study. New England Journal of Medicine 1989;321:1009–14.
[54] Guirguis EM, Barber GG. The natural-history of abdominal aortic-aneurysms. American Journal of Surgery 1991;162:481–3.
[55] Mohan S, Mohan N, Valente AJ, Sprague EA. Regulation of low shear flow-induced haec vcam-1 expression and monocyte adhesion. American Journal of Physiology-Cell Physiology 1999;276:C1100–7.
[56] Walpola PL, Gotlieb AI, Langille BL. Monocyte adhesion and changes in endothelial-cell number, morphology, and f-actin distribution elicited by low shear-stress invivo. American Journal of Pathology 1993;142:1392–400.
[57] Jou LD, Wong G, Dispensa B, Lawton MT, Higashida RT, Young WL, et al. Correlation between lumenal geometry changes and hemodynamics in fusiform intracranial aneurysms. American Journal of Neuroradiology 2005;26:2357–63.
[58] Platt MO, Ankeny RF, Jo HJ. Laminar shear stress inhibits cathepsin l activity in endothelial cells. Arteriosclerosis Thrombosis and Vascular Biology 2006;26:1784–90.
[59] Nissen R, Cardinale GJ, Udenfriend S. Increased turnover of arterial collagen in hypertensive rats. Proceedings of the National Academy of Sciences of the United States of America 1978;75:451–3.
[60] Malek AM, Izumo S. Control of endothelial cell gene expression by flow. Journal of Biomechanics 1995;28:1515–28.
[61] Rizvi MAD, Katwa L, Spadone DP, Myers PR. The effects of endothelin-1 on collagen type i and type iii synthesis in cultured porcine coronary artery vascular smooth muscle cells. Journal of Molecular and Cellular Cardiology 1996;28:243–52.
[62] Chiu JJ, Chen LJ, Lee PL, Lee CI, Lo LW, Usami S, et al. Shear stress inhibits adhesion molecule expression in vascular endothelial cells induced by coculture with smooth muscle cells. Blood 2003;101:2667–74.
[63] Allaire E, Forough R, Clowes W, Starcher B, Clowes AW. Local overexpression of timp-1 prevents aortic aneurysm degeneration and rupture in a rat model. Journal of Clinical Investigation 1998;102:1413–20.
[64] Crowther M, Goodall S, Jones JL, Bell PRF, Thompson MM. Increased matrix metalloproteinase 2 expression in vascular smooth muscle cells cultured from abdominal aortic aneurysms. Journal of Vascular Surgery 2000;32:575–83.
[65] Curci JA. Digging in the "Soil" Of the aorta to understand the growth of abdominal aortic aneurysms. Vascular 2009;17:S21–9.
[66] Patel MI, Melrose J, Ghosh P, Appleberg M. Increased synthesis of matrix metalloproteinases by aortic smooth muscle cells is implicated in the etiopathogenesis of abdominal aortic aneurysms. Journal of Vascular Surgery 1996;24:82–92.
[67] Sumpio BE, Banes AJ, Link WG, Johnson JG. Enhanced collagen production by smooth muscle cells during repetitive mechanical stretching. Archives of Surgery 1988;123:1233–6.
[68] Doyle BJ, Callanan A, Burke PE, Grace PA, Walsh MT, Vorp DA, et al. Vessel asymmetry as an additional diagnostic tool in the assessment of abdominal aortic aneurysms. Journal of Vascular Surgery 2009;49:443–54.
[69] Vorp DA, Raghavan ML, Webster MW. Mechanical wall stress in abdominal aortic aneurysm: Influence of diameter and asymmetry. Journal of Vascular Surgery 1998;27:632–9.
[70] Mantha A, Karmonik C, Benndorf G, Strother C, Metcalfe R. Hemodynamics in a cerebral artery before and after the formation of an aneurysm. American Journal of Neuroradiology 2006;27:1113–8.
[71] Himburg HA, Dowd SE, Friedman MH. Frequency-dependent response of the vascular endothelium to pulsatile shear stress. American Journal of Physiology-Heart and Circulatory Physiology 2007;293:H645–53.
[72] Chappell DC, Varner SE, Nerem RM, Medford RM, Alexander RW. Oscillatory shear stress stimulates adhesion molecule expression in cultured human endothelium. Circulation Research 1998;82:532–9.
[73] Conway DE, Williams MR, Eskin SG, McIntire LV. Endothelial cell responses to atheroprone flow are driven by two separate flow components: low time-average shear stress and fluid flow reversal. American Journal of Physiology-Heart and Circulatory Physiology 2010;298:H367–74.
[74] Sorescu GP, Sykes M, Weiss D, Platt MO, Saha A, Hwang J, et al. Bone morphogenic protein 4 produced in endothelial cells by oscillatory shear stress stimulates an inflammatory response. Journal of Biological Chemistry 2003;278:31128–35.
[75] Wang C, Garcia M, Lu X, Lanir Y, Kassab GS. Three-dimensional mechanical properties of porcine coronary arteries: a validated two-layer model. American Journal of Physiology-Heart and Circulatory Physiology 2006;291:H1200–9.